A Simulated Study of Close Contacts in Pedestrian Models

Charles Tang
Algonquin Regional High School
Northborough, Massachusetts, USA

Archanaa S. Krishnan
Virginia Tech
Blacksburg, Virginia, USA

Patrick Schaumont
Worcester Polytechnic Institute
Worcester, Massachusetts, USA

ABSTRACT

A simulation-based study was designed to compare close contacts in one-way hallways, two-way hallways, and rooms. Our simulations examine the effects of the number of pedestrians, environment size, walking speed, and contact radius using an anticipatory pedestrian interaction model. We reproduce the original study and extend it with an explicitly timed, seeded simulation environment. The main experiment includes 396 parameter combinations and 3,960 trajectories, with ten repetitions per combination. For the subset with density at most 2 pedestrians/m^2, one-way movement reduces the number of unique contacting pairs by 73.08% relative to two-way movement, but reduces summed contact time per person by only 5.91%. We derive a spatial-mixing relationship in which contact time per person is proportional to density, observation time, and the square of the contact radius. Additional experiments test this relationship, the effect of observation duration, and the numerical sensitivity of crowded scenarios. These results explain why fewer distinct contacts do not imply an equally large reduction in cumulative contact time. They support evaluating pedestrian arrangements with multiple contact measures. The simulations measure proximity and do not estimate infections or establish a safe occupancy limit.

CCS CONCEPTS

• **Computing methodologies** → **Agent / discrete models**; • **Applied computing** → *Health care information systems.*

KEYWORDS

pedestrian movement, crowd simulation, close contacts, contact duration, density, COVID-19

1 INTRODUCTION

The COVID-19 pandemic raised questions about how schools and other buildings should organize pedestrian movement. One-way hallways, occupancy limits, and changes to the use of shared spaces were considered as ways to reduce close interactions. Building design and operation can influence opportunities for exposure, although the effects of a change depend on the transmission mechanism being considered [Dietz et al. 2020]. A hallway arrangement should therefore be evaluated by what it changes in pedestrian interactions and by what the experiment can actually measure.

One-way movement can reduce encounters between pedestrians traveling in opposite directions. However, pedestrians traveling together may remain near one another for a longer period of time. This creates two separate questions: how many different people does a pedestrian encounter, and how much total time is spent near other people? A model that records only one of these measurements may give an incomplete comparison. Mathematical work on academic buildings has also identified the importance of time spent in transit when comparing one-way and two-way routes [Romero et al. 2020].

The purpose of this paper is to compare one-way hallway, two-way hallway, and room scenarios using simulated pedestrian environments. We use the term *hallway* to describe the direction of movement. The underlying environment is a periodic square, rather than a building corridor with walls, doors, and destinations. This allows us to study movement direction at a controlled population and area. It also limits what can be concluded about an actual hallway network.

The original poster reported 68.62% fewer close contacts for a one-way hallway [Tang et al. nd]. The accompanying manuscript contained preliminary figures and an unfinished analysis. In this study, we preserve those materials, examine the available source code, and run a new set of reproducible experiments. We correct the difference between the time used to update pedestrian motion and the time assigned to a recorded contact. We also separate the radius used to observe contacts from the radius used to select neighbors for collision avoidance. The new results are reported separately from the historical poster summary.

Our study makes three contributions. First, it compares the number of contacting pairs, cumulative time per contacting pair, and summed contact time per person within the same experiments. Second, it derives mathematical relationships that explain the different effects of density, speed, and movement direction on these measurements. Third, it tests these relationships with additional experiments and numerical checks. Our results show that movement direction has a much larger effect on the number of distinct contacts than on total contact time. This distinction is necessary before proximity results can be used in a model of viral exposure.

2 RELATED WORK

2.1 Pedestrian movement

Pedestrian simulations describe how individual movement produces crowd patterns. Experiments with corridors, bottlenecks, and intersections have shown that geometric boundaries influence pedestrian flow and self-organization [Helbing et al. 2005]. These results motivate the use of simulations, but also show why a periodic square cannot represent every feature of a building.

Karamouzas et al. proposed an anticipatory interaction model based on the projected time to a potential collision [Karamouzas et al. 2014]. Their model reproduced several observed crowd phenomena. We use the interaction equation implemented in the original project as a common movement rule across scenarios. The ability of that model to reproduce crowd patterns does not independently validate the present contact measurements or its use for infection prediction.

2.2 Movement and exposure

Romero et al. modeled one-way and two-way foot traffic within an academic building [Romero et al. 2020]. Their analysis considered distance-dependent exposure and travel time, including the possibility that a one-way route increases the time required to reach a destination. Our experiment instead holds the observation period and population fixed. The two approaches address different parts of the same problem: local interaction patterns and complete routes through a building.

Shumsky et al. combined customer movement with direct and wake exposure models in retail stores [Shumsky et al. 2021]. Their work showed that the effect of one-way movement depends on the exposure mechanism. We do not assign infectious states or use a transmission kernel. Our comparison concerns the contact patterns that such a model would receive as inputs.

Airflow studies provide a further reason to distinguish proximity from infection. Vuorinen et al. simulated aerosol transport and accumulation of inhaled exposure in indoor environments [Vuorinen et al. 2020]. Bazant and Bush developed an indoor airborne transmission model that includes occupancy, exposure time, and removal of infectious aerosol [Bazant and Bush 2021]. Engineering controls such as ventilation and filtration are also discussed by Morawska et al. [Morawska et al. 2020]. None of these processes is represented by a fixed geometric contact radius. Our contact results therefore describe one component of a broader exposure problem.

3 SIMULATION METHODOLOGY

3.1 Pedestrian interactions

Our simulation uses a Python implementation of the anticipatory power-law model described by Karamouzas et al. [Karamouzas et al. 2014; Tang 2021]. Its interaction potential is

$$E(\tau) = \frac{k}{\tau^2}\exp(-\tau/\tau_0), \qquad \mathbf{F}_{ij} = -\nabla_{\mathbf{r}_i} E(\tau_{ij}), \tag{1}$$

where τ_{ij} is the projected time to collision for a pair of pedestrians. We retain $k = 1.5$, $\tau_0 = 3$ s, a nominal pedestrian radius of 0.2 m, and the original limit of 5 m/s^2 on each pair's avoidance acceleration. Each pedestrian also relaxes toward a preferred velocity with a 0.5 s relaxation time. The original uniform perturbation in each coordinate, between -1 and 1 m/s^2, is retained.

The original code scales each initial velocity by a factor of 1.5 to obtain the preferred velocity. Consequently, a speed factor v of 0.5, 1, 1.5, or 2 corresponds to a preferred speed of 0.75, 1.5, 2.25, or 3 m/s. These are input preferences. Avoidance changes the realized walking speed, which we record separately.

The implementation is an adaptation of an existing model. In particular, its neighborhood cutoff and its treatment of overlapping pedestrians are retained for comparison with the original experiments. It reduces the effective collision radius when pedestrians overlap, rather than enforcing a hard body constraint. We return to the implications of this choice when discussing dense scenarios.

3.2 Environment and scenarios

Pedestrians move in a square of side length s and area $A = s^2$. Both coordinates are periodic. Distances and avoidance displacements use the nearest periodic image. In the corrected implementation, a pedestrian who crosses a boundary retains the excess displacement through a modulo operation. There are no entrances, exits, or physical dividing barriers.

Initial positions are uniformly distributed over the square. We compare the following movement scenarios, using the original angular spread $a = 0.2$ radians.

Room. Initial directions are uniformly distributed over $[0, 2\pi)$. This represents movement without a common direction, rather than a room with specific activities or destinations.

One-way hallway. Initial directions are uniformly distributed over $[\pi - a, \pi + a]$. All pedestrians have approximately the same preferred direction.

Two-way hallway. Initial directions are distributed around either 0 or π. To retain the original soft separation, pedestrian i is assigned the direction around π when

$$y_i \geq s/2 - Z_i, \tag{2}$$

where Z_i is drawn independently and uniformly from the integers $-b, \ldots, b-1$, with $b = \lfloor 3s/5 \rfloor$. Otherwise, the direction is assigned around 0. This produces overlapping directional streams, rather than two enforced lanes. Direction assignment is based on the initial position and is not continually reassigned during movement.

3.3 Time and contact recording

The archived implementation advanced movement by 0.02 s per update, recorded contacts every update, and assigned 0.1 s to each record. It stopped after 601 records. These settings represent 12.02 s of motion and 60.1 s of assigned contact weight. The physical contact time associated with those records is one fifth of the reported time. This difference affects both the interpretation of contact duration and the observation horizon.

Our main experiments measure 60 physical seconds, sample contacts every 0.1 s, and integrate movement with a 0.005 s time step. The perturbing acceleration is held constant within each 0.02 s interval so that refinements of the integration step use the same forcing path. Samples at $t = 0, 0.1, \ldots, 59.9$ s are weighted by 0.1 s. This is a left-rectangle approximation of cumulative contact time. We also retain a separately labeled diagnostic using the original 601-frame convention.

For a contact radius r, a pair is observed when the periodic center-to-center distance is strictly less than r. The main avoidance neighborhood has radius $R_a = 1$ m. Contact radii of 1, 1.5, 2, 2.5, and 3 m are observed on the *same trajectories*. Changing the observation radius therefore changes the measurement without changing pedestrian behavior. A separate experiment changes R_a to 3 m.

3.4 Outcome measures

Let $X_{ij}(t)$ indicate whether unordered pair $i < j$ is within the contact radius at time t. Over an observation period T, define

$$d_{ij} = \int_0^T X_{ij}(t)\, dt, \tag{3}$$

$$C = \sum_{i<j} \mathbf{1}\{d_{ij} > 0\}, \qquad D = \sum_{i<j} d_{ij}. \tag{4}$$

Here, C is the number of unique contacting pairs and D is total pair-seconds. A pair that meets more than once contributes once to C, while all of its observed contact time contributes to D.

The mean cumulative contact time among contacting pairs is

$$\bar{t} = \frac{D}{C}, \qquad C > 0. \tag{5}$$

If I is the number of unordered pair observations and Δt is the observation interval, then $D = I\Delta t$. Thus, $\bar{t} = I\Delta t/C$. This corrects the inverted expression in the preliminary manuscript. It is cumulative time per contacting pair, rather than the duration of a single uninterrupted encounter. Runs with no contacting pairs would have an undefined conditional mean.

To compare different population sizes, we also calculate mean distinct contacts per person, $2C/N$, and summed contact time per person,

$$B = \frac{2D}{N}. \tag{6}$$

The factor of two assigns each pair's time to both pedestrians. A pedestrian can be close to several people at once, so B may exceed T. It is a sum of contact durations, not time spent in a binary exposed state. Equivalently, B/T is the time-average number of neighbors within the contact radius, averaged over pedestrians.

3.5 Experimental design and analysis

The main parameter grid is shown in Table 1. The listed movement, size, population, and speed settings produce 396 combinations. The five observation radii do not create additional independent trajectories. The preliminary draft's count of 792 combinations cannot be reconstructed from its listed grid, so it is not used as a verified historical run count.

We use ten fixed seeds for each combination. Within a combination, the three movement scenarios share initial positions and the underlying forcing draws. The new random-number generator does not recreate the unknown seeds of the historical experiments. We verified the headless implementation against the archived scalar force and update functions on controlled states.

For a measurement Y, we report the one-way reduction relative to two-way movement as

$$R_Y = 100\left(1 - \frac{\sum Y_{\text{one}}}{\sum Y_{\text{two}}}\right). \tag{7}$$

The sums include the same settings and seeds. This is a ratio of sums, rather than an unweighted mean of the percentage change in each setting. Larger baseline outcomes contribute more to the ratio. We estimate 95% percentile intervals using 10,000 paired bootstrap resamples of the ten seed blocks. Each block preserves all settings and movement scenarios for that seed. These intervals describe variation from initialization and forcing within the specified simulation model. They do not describe uncertainty about real pedestrian behavior or disease transmission.

Numerical checks found that the densest cases remained sensitive to the integration step. We therefore emphasize the subset with $\rho \le 2$ pedestrians/m^2, which contains 112 settings per movement model and 3,360 trajectories. We report the full grid as a computational stress test. This restriction followed the numerical checks and is not evidence that a density of 2 is a general physical or epidemiological threshold.

4 MATHEMATICAL RELATIONSHIPS

4.1 Contact counts and contact time

The definitions above give the exact relationship

$$D = C\bar{t}, \qquad B = \frac{2C\bar{t}}{N}. \tag{8}$$

For matched populations, the ratio between two movement scenarios is therefore

$$\frac{B_1}{B_2} = \frac{C_1}{C_2}\frac{\bar{t}_1}{\bar{t}_2}. \tag{9}$$

A reduction in the number of contacts can be offset by an increase in cumulative time with the remaining contacts. This identity applies to each matched run. Products of separately averaged table entries need not satisfy it, because averaging does not preserve a product.

This also affects the interpretation of correlations. If mean contact time is defined as D/C, a negative association between C and $\bar{t}$ is partly built into the measurements. It is not independent evidence that one movement model causes a particular exposure response. We use D and B to examine whether a lower pair count corresponds to a lower cumulative burden.

4.2 Density and contact radius

A useful reference case assumes that pedestrian positions are independently and uniformly mixed over area A. On a square torus, if $r \le s/2$, the probability that a specified pair is within radius r at any fixed time is

$$p_r = \frac{\pi r^2}{A}. \tag{10}$$

Linearity of expectation then gives

$$\mathbb{E}[D] = \binom{N}{2}\frac{\pi r^2}{A}T, \qquad \mathbb{E}[B] = \pi r^2 T\frac{N-1}{A}. \tag{11}$$

Temporal samples do not need to be independent for this expectation. The condition is a uniform independent spatial distribution of each pair at each time. For larger r, the disk intersects its periodic images and the available area must be calculated using the torus geometry instead of πr^2.

Using $\rho = N/A$, Eq. 11 becomes

$$\mathbb{E}[B] = \pi r^2 T\rho\left(1 - \frac{1}{N}\right). \tag{12}$$

This predicts an approximately linear relationship with density and a quadratic relationship with the observation radius. It also predicts approximately the same burden when population and area increase together at fixed density. At fixed area, however, total pair-seconds grow as $N(N-1)$, while per-person burden grows as $N-1$. Total contacts should therefore not be interpreted without accounting for the number of possible pairs.

For an interacting crowd, we can write the more general expression

$$\mathbb{E}[B] = \frac{N-1}{A}\int_0^T \int_{\|\mathbf{z}\|<r} g(\mathbf{z}, t)\, d\mathbf{z}\, dt, \tag{13}$$

where g is the pair separation density relative to uniform independent positions. Avoidance, crowding, and directional organization can change g. Equation 12 is the special case $g = 1$, not a universal law for all crowds.

Table 1: Main experimental design. Density is derived from population and area. Contact radii are observation settings applied to the same trajectories.

Parameter	Values or definition
Movement	Room, one-way hallway, two-way hallway
Side length s (m)	5, 7.5, 10, 12.5, 15, 17.5, 20, 22.5, 25, 27.5, 30
Population N	100, 150, 200
Speed factor v	0.5, 1, 1.5, 2; preferred speed $1.5v$ m/s
Density ρ	N/s^2, ranging from approximately 0.111 to 8 pedestrians/m^2
Observation radius r (m)	1, 1.5, 2, 2.5, 3
Avoidance radius R_a	1 m in the main experiment; 3 m in a separate sensitivity experiment
Time	60 s observed; 0.005 s integration step; 0.1 s contact samples; no initial warm-up in the main experiment
Repetitions	Ten seeds, 202100–202109, paired across movement scenarios
Main size	$3 \times 11 \times 3 \times 4 = 396$ movement/size/population/speed combinations; 3,960 trajectories and 19,800 radius-specific observations

We test a power-law approximation in the dilute subset $\rho \le 0.5$:

$$\log(B/T) = \beta_0 + \beta_\rho \log\left(\frac{N-1}{A}\right) + \beta_r \log r + \beta_v \log v. \tag{14}$$

The spatial-mixing reference predicts $\beta_\rho = 1$, $\beta_r = 2$, and $\beta_v = 0$. We fit the means of the ten runs for each setting, rather than treating pair observations as independent data. Prediction is checked by leaving out one environment side length at a time. These checks test interpolation within the simulation design, not transfer to a building.

4.3 Relative velocity and passing time

The relative speed of two pedestrians with the same speed u and directional difference $\Delta\theta$ is

$$u_{\text{rel}} = 2u\,|\sin(\Delta\theta/2)|\,. \tag{15}$$

Pedestrians moving in opposite directions can therefore meet more new people, while pedestrians moving together can remain close for longer. For two independent headings uniformly distributed within an interval of half-width a, integration over their triangular difference distribution gives

$$\mathbb{E}[u_{\text{rel}}]_{\text{one}} = \frac{4u(a - \sin a)}{a^2}. \tag{16}$$

At $a = 0.2$, this is approximately $0.1331u$. Uniform directions over the circle give $4u/\pi \approx 1.2732u$. For independently mixed, equally likely opposing streams, the expected relative speed is

$$\frac{1}{2}\frac{4u(a - \sin a)}{a^2} + u\left(\frac{\sin(a/2)}{a/2}\right)^2 \approx 1.0632u. \tag{17}$$

This last reference assumes independent directions and positions. It does not reproduce the spatially correlated soft separation or the changing velocities of our interacting two-way model.

For straight motion, the relative path of a pair sweeps a region consisting of an initial disk plus a strip of width $2r$. Before the path overlaps itself on the torus, its expected area is $\pi r^2 + 2r\mathbb{E}[u_{\text{rel}}]T$. Thus,

$$\mathbb{E}[C] \approx \binom{N}{2}\frac{\pi r^2 + 2r\mathbb{E}[u_{\text{rel}}]T}{A}. \tag{18}$$

The expression applies to straight trajectories with no self-overlap of the swept region. It cannot continue growing past $\binom{N}{2}$. Avoidance, repeated contacts, and a longer observation period change the approximation.

For an isolated straight crossing with perpendicular separation $b < r$, the contact duration is

$$t_{\text{pass}} = \frac{2\sqrt{r^2 - b^2}}{u_{\text{rel}}}. \tag{19}$$

A larger relative speed increases the area swept per unit time but decreases the duration of each crossing. Under uniform spatial mixing, these effects compensate in the expectation for D. This explains why speed can change contact counts and pair durations more than it changes total contact time. A cumulative pair time in a periodic environment can include several such crossings and is not equal to one passing time.

5 RESULTS

5.1 Comparison of movement scenarios

For $\rho \le 2$, one-way movement reduces unique contacting pairs by 73.08% compared with two-way movement, with a seed-bootstrap 95% interval of 72.84%–73.31%. The reduction in summed contact time per person is 5.91%, with an interval of 5.18%–6.62%. The difference between these effects is central to the comparison: one-way movement repeatedly places pedestrians near a smaller set of people.

Table 2 summarizes the three scenarios. Room movement produces more contacts than the directional models in the aggregate, while one-way movement has longer cumulative time per contacting pair. The room's mean summed time per person, 116.21 s, is slightly below the two-way value of 118.28 s despite its higher contact count. Thus, even the ordering of scenarios depends on the measurement being compared. These patterns do not establish an ordering of infection probabilities, which would require an exposure and transmission model.

Table 2: Mean measurements over the lower-density subset ($\rho \leq 2$), with 112 parameter settings and ten seeds per movement scenario. Pair time is conditional on the pair having contacted. Time/person is summed across simultaneous contacts and can exceed 60 s.

Movement	Unique pairs	Pair time (s)	Time/person (s)	Speed (m/s)
Room	5,852.1	1.49	116.21	1.65
One-way	1,103.4	8.03	111.29	1.87
Two-way	4,098.3	2.24	118.28	1.69

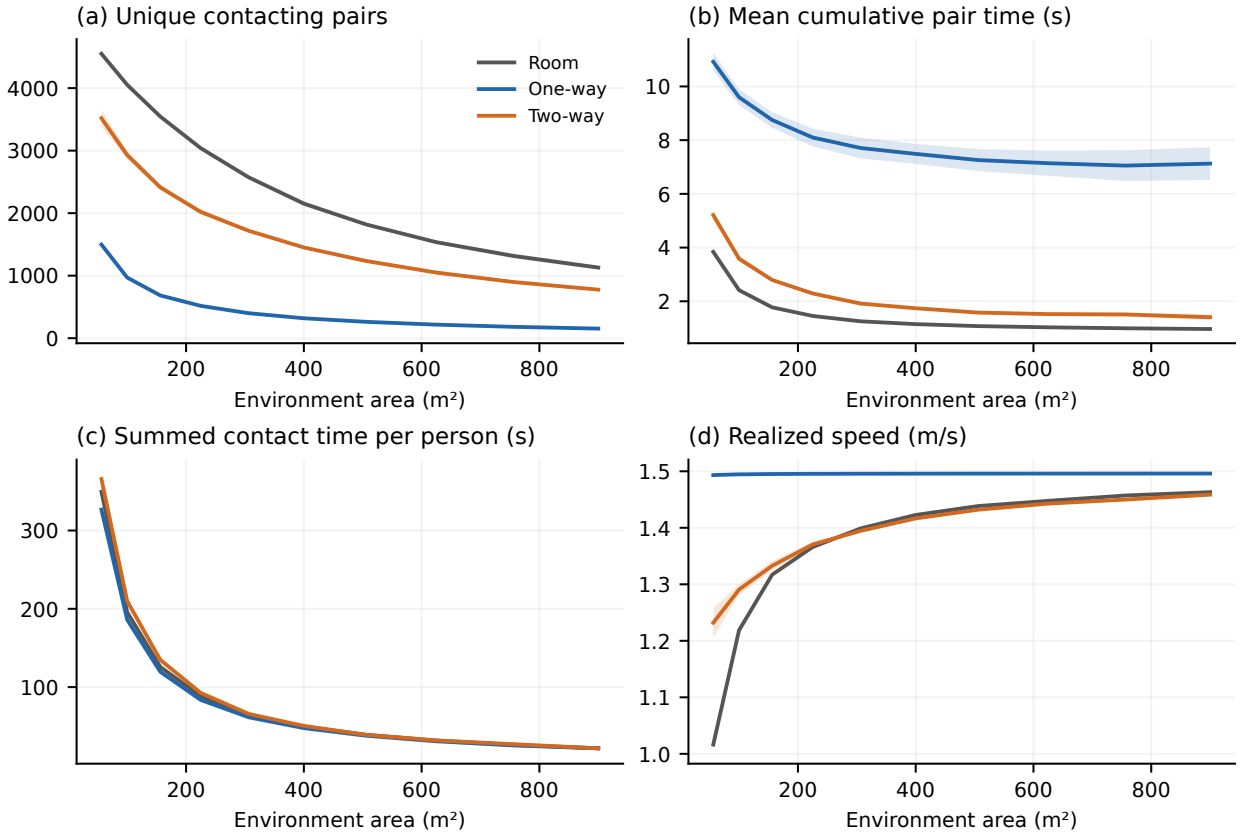

Figure 1: Effect of environment area for 100 pedestrians and speed factor 1. Curves show means of ten runs; shaded bands show 95% t intervals across seeds. Unique pairs, conditional pair time, summed time/person, and realized speed describe different aspects of the same trajectories.

5.2 Effect of environment size and density

Increasing area at fixed population reduces contact opportunities. Figure 1 shows that the number of unique contacts and summed time per person decrease with increasing area. The mean cumulative duration among the remaining contacting pairs changes less once the environment is sufficiently dilute. This reproduces the qualitative distinction in the original poster: the number of contacts can continue decreasing after conditional pair time appears to level off.

The mathematical interpretation is that the two measurements have different denominators. Both the amount of contact time and the number of pairs contributing that time can decrease together. Their ratio may then change little. A plateau in $\bar{t}$ therefore does not imply that extra space has no benefit, and it does not identify a density below which transmission is safe. An apparent plateau also depends on speed, contact radius, movement scenario, and the finite observation period.

5.3 Effect of walking speed

Figure 2 compares speed factors in one-way and two-way movement. Increasing preferred speed generally produces more distinct contacting pairs while reducing cumulative time per contacting pair.

The effect on summed contact time is smaller. The relative-velocity and passing-time relationships explain this combination without requiring a change in the geometric probability of close proximity.

We also fit within-setting log–log slopes at $r = 1$ and $\rho \leq 0.5$, removing a separate intercept for each population, area, and seed. For one-way movement, the fitted speed exponents are 0.699 for C, -0.686 for $\bar{t}$, and 0.013 for D. The corresponding two-way exponents are 0.798, -0.796, and 0.002. The near cancellation is consistent with Eq. 8. It is an explanatory fit over the tested speeds, rather than a general speed law or an independent confirmation of the algebraic identity.

These measurements concern a fixed period in a periodic environment. They cannot show that increasing walking speed lowers exposure over a complete trip. A faster trip, a longer one-way detour, and congestion at a destination would change the observation time and the set of interactions. Those quantities are absent from the present environment.

5.4 Empirical scaling of contact time

Table 3 reports the fitted exponents in Eq. 14. Across movement models, the density exponents range from 0.993 to 1.017 and the radius exponents range from 1.960 to 1.990. The absolute speed exponents are below 0.013. Median prediction errors for held-out side lengths range from approximately 0.50% to 1.00%. These results support the spatial-mixing approximation within the dilute part of this simulation design. The held-out errors are reported alongside the in-sample fit because a large R^2 alone does not establish predictive value.

The fitted radius relationship concerns the observation rule. Increasing r includes more pairs and more of each pair's trajectory. It does not cause a pedestrian to alter their movement because the avoidance radius is held fixed. Figure 3 shows the resulting measurement sensitivity. A radius-dependent result should always specify the radius and the separate movement assumptions.

5.5 Additional experiments

We performed three sets of additional experiments to separate mathematical relationships from features of the interacting model. First, ideal-motion controls remove avoidance and random forcing. They use constant speeds of 0.75, 1.5, and 3 m/s, 100 pedestrians in a 20 m square, contact radii of 0.5, 1, and 2 m, and a 2 s observation period. The two-way control assigns directions independently of position, as assumed by Eq. 17. Thirty seeds per movement/speed setting produce 270 trajectories and 27 radius-specific condition means. The finite-sample swept-area prediction uses a path ending at 1.98 s, while contact time retains the full 2 s weight. Across these conditions, the mean absolute percentage errors are 2.34% for unique pairs and 2.23% for summed time per person. The largest errors are approximately 10.4% and 10.5%, respectively. The controls support the limiting calculation and do not validate human behavior.

Second, matched-density experiments vary N over 50, 100, and 200 and set $s = \sqrt{N/\rho}$ for densities of 0.25, 0.5, 1, and 2. All movement models use speed factor 1, with ten seeds. These experiments directly test the prediction that per-person burden changes little when population and area increase together. The finite-population factor in Eq. 12 predicts a ratio of $199/196 \approx 1.015$ between the 200-person and 50-person cases at equal density. Measured deviations from this reference also include avoidance and finite-domain effects.

Across the twelve movement/density comparisons, the observed 200-person to 50-person burden ratios range from 0.975 to 1.064. This is much closer to a constant per-person burden than to a fourfold increase. It supports density as the useful explanatory variable when area increases with population, while allowing departures from the independent-mixing approximation (Figure 4c).

Third, observation-horizon experiments use 1, 5, 12, 30, 60, and 120 s for 100 pedestrians at speed factor 1 in squares of side 10 and 20 m. Ten paired seeds are used per setting. Unique-pair counts depend on the observation horizon because a pair is counted only once, even if it meets again. Total pair-seconds continue accumulating during repeated contacts. As a result, a percentage reduction in distinct contacts is a property of the chosen observation window, rather than a fixed characteristic of a movement rule.

In this subset, the one-way reduction in unique pairs changes from 31.38% at 1 s to 70.59% at 60 s and 68.65% at 120 s. The corresponding time/person reductions are -1.80%, 10.23%, and 12.23%. The 95% interval for the 1 s time/person contrast includes zero reduction, whereas the 60 s and 120 s intervals are positive. At 5 s, one-way movement has 2.60% greater time/person, with a seed-bootstrap interval for the reduction of $[-5.36, -0.54]$%. This short-horizon counterexample shows why the observed reduction in contacts should not be generalized to every observation window or outcome.

5.6 Numerical and model sensitivity

We compare integration steps of 0.02, 0.01, 0.005, and 0.0025 s in a matched subset with 100 pedestrians, side lengths 5, 10, and 20 m, speed factors 0.5, 1, and 2, and ten seeds for each movement model. The same 0.02 s forcing path is used at every step size. Additional stress tests use 150 and 200 pedestrians in a 5 m square and steps as small as 0.00125 s. A boundary check uses 200 pedestrians in a 10 m square ($\rho = 2$), all four speed factors, and ten seeds per movement model, comparing 0.005 with 0.0025 s. These tests distinguish variability between seeds from sensitivity to the numerical method.

The largest integration effects occur in the crowded scenarios. In the 5 m stress subset with 150 or 200 pedestrians, the pair-count reduction changes from 61.08% at a 0.005 s step to 45.59% at 0.0025 s and 40.60% at 0.00125 s. These changes are much larger than the seed-bootstrap intervals. They make a universal claim that one-way movement is safest in the narrowest or densest environment unsupported by the present model. These cases should be interpreted as numerical stress tests. The lower-density scaling analysis is more stable and does not rely on them.

Within the lower-density part of the 100-person step-size subset, halving the step from 0.005 to 0.0025 s changes the aggregate pair-count reduction from 68.78% to 68.71%. The time/person reduction changes from 5.74% to 4.66%, with overlapping seed-bootstrap intervals. Across the individual movement/size/speed settings in that subset, the largest changes in ten-run means are 0.78% for contact counts and 2.38% for time/person. This provides a numerical check for that subset and does not establish convergence throughout the dense grid.

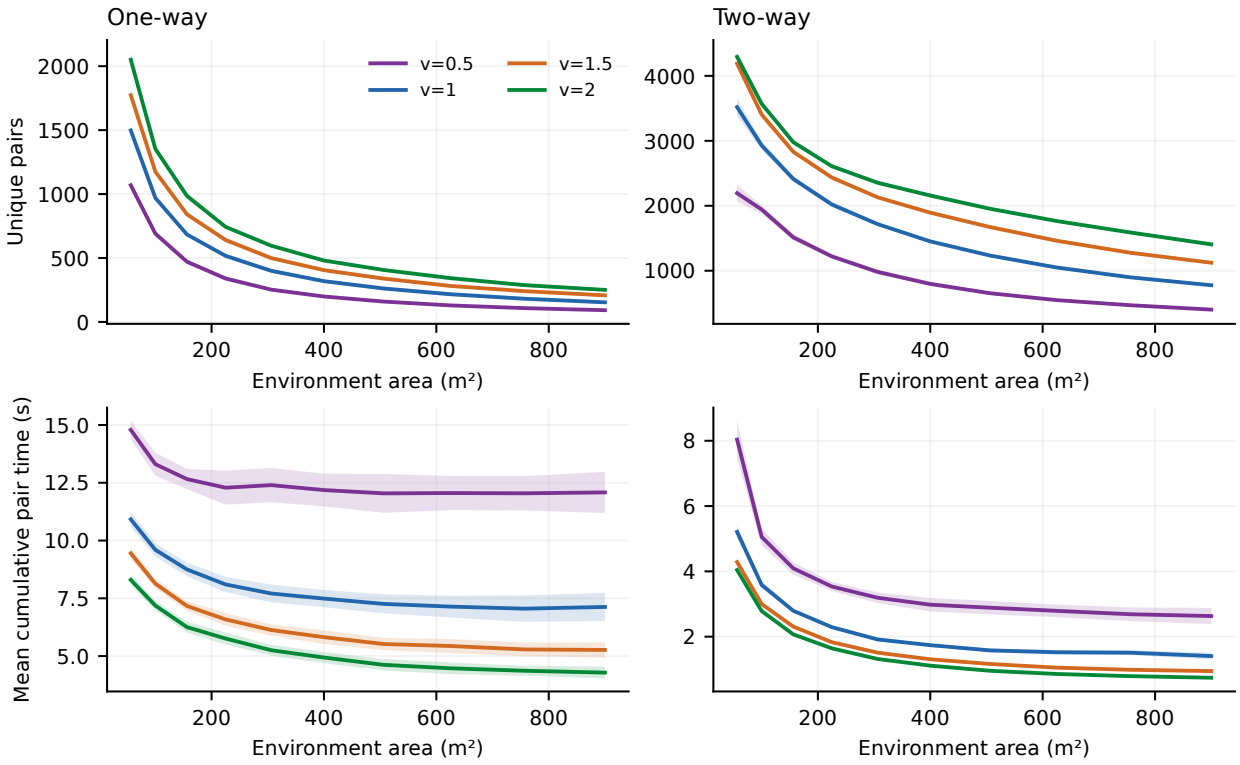

Figure 2: Effect of preferred speed on unique pair counts and mean cumulative pair time for 100 pedestrians. The input factor v corresponds to preferred speed $1.5v$ m/s. Bands are 95% t intervals across ten seeds.

Table 3: Power-law fit for $\rho \leq 0.5$, using 360 radius-specific condition means per movement scenario. CV error is the median absolute percentage error when an entire side length is held out. The dependent variable is $\log(B/T)$.

Movement	β_ρ	β_r	β_v	$R^2_{\log}$	CV error (%)
Room	0.999	1.960	0.0128	0.99990	0.52
One-way	0.993	1.990	-0.0009	0.99985	0.50
Two-way	1.017	1.970	-0.0004	0.99967	1.00

At the $\rho = 2$ boundary, the pair-count reduction changes from 63.96% to 63.93% under the same refinement, and the time/person reduction changes from 7.38% to 7.37%. The largest changes in condition means are 2.53% and 1.97%, respectively. These results support the lower-density interpretation while leaving the much denser stress cases unresolved.

We also test a 3 m avoidance neighborhood and a 10 s warm-up followed by 60 s of observation in the matched 100-person subset. These are changes to behavior or initialization, rather than changes to the contact definition. Increasing the avoidance neighborhood changes the pair-count reduction from 54.14% to 47.24%, while the 10 s warm-up changes it to 53.29%. Table 4 reports the corresponding time results and intervals. The comparison includes the numerically sensitive 5 m square, so it demonstrates dependence on the model assumptions without establishing a converged dense-crowd estimate.

6 DISCUSSION

6.1 Interpreting the original findings

The original poster identified a useful qualitative result: aligned movement can reduce the number of different people encountered. Our new experiments support that interpretation. They also show why the reported reduction in contacts should not be described as the same reduction in viral risk. One-way movement produces a smaller set of contacts, but contact with that set lasts longer. Equations 8 and 9 state the relationship directly.

The historical 68.62% reduction cannot be independently reconstructed from the poster and available summary figures. Its original aggregation weights and complete run-level data are unavailable. With new seeds, our full-grid diagnostic using the original 601-frame convention gives 66.57% fewer pairs, with a seed-bootstrap interval of 66.08%–67.04%. The refined full-grid estimate is 68.39%,

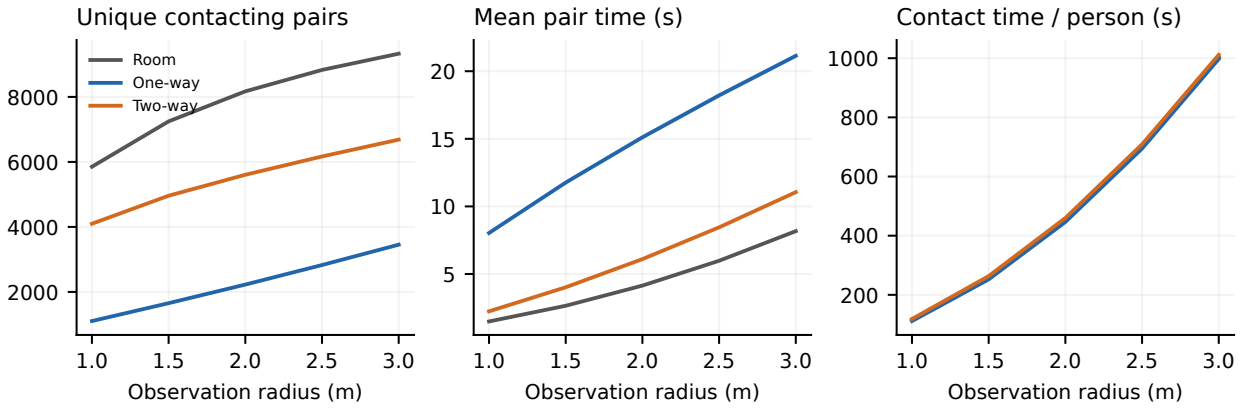

Figure 3: Sensitivity to observation radius on the same lower-density main trajectories ($\rho \leq 2$). Each plotted value first averages over that parameter grid within a seed. Shading shows a 95% t interval over the ten seed summaries. The avoidance neighborhood remains fixed at 1 m.

Table 4: Sensitivity comparisons, with 95% seed-bootstrap intervals in brackets. The avoidance and warm-up subset uses $N = 100$, $s = 5, 10, 20$ m, and speed factors 0.5, 1, 2. Its matched baseline includes the same settings, including the dense 5 m case, and should not be directly compared with the main lower-density percentage. The step-size rows use the lower-density part of that subset.

Experiment	Grid	Pair reduction (%)	Time/person reduction (%)
Main, dt=0.005 s	$\rho \leq 2$	73.08 [72.84, 73.31]	5.91 [5.18, 6.62]
Matched baseline	Avoidance subset	54.14 [53.26, 54.87]	4.26 [3.55, 4.90]
Avoidance radius 3 m	Same subset	47.24 [46.29, 48.28]	5.67 [4.20, 7.22]
Matched baseline	Warm-up subset	54.14 [53.26, 54.87]	4.26 [3.55, 4.90]
Warm-up 10 s	Same subset	53.29 [52.28, 54.22]	4.55 [3.93, 5.13]
Step 0.005 s	$N = 100$, $s = 10, 20$ m	68.78 [68.38, 69.14]	5.74 [4.27, 7.51]
Step 0.0025 s	$N = 100$, $s = 10, 20$ m	68.71 [68.27, 69.13]	4.66 [2.26, 6.88]

but includes dense stress cases; the lower-density estimate is 73.08%. These percentages use explicitly defined experiments and are not estimates of the same historical quantity. Agreement in the qualitative trend is useful, but numerical differences should not be attributed to a single cause when the horizon, initialization, time step, and aggregation can all matter.

The poster also suggested that more pedestrians could move through a one-way environment without a significant increase in risk. Our periodic experiment does not measure throughput: nobody enters, reaches a destination, or leaves. At fixed area, increasing population increases the number of possible pairs and the expected contact burden. At fixed density, increasing population together with area has a different effect. These are separate comparisons, and neither establishes a safe building capacity.

6.2 What the relationships suggest

The density relationship provides a straightforward way to interpret changes in occupancy and space. Under the spatial-mixing assumptions, doubling area at fixed population halves expected contact time per person. Doubling population at fixed area approximately doubles per-person burden and approximately quadruples total pair-seconds. Doubling the observation radius approximately quadruples the measured burden. These are model-based scaling statements, rather than recommendations that a particular density or distance prevents infection.

The speed relationship explains another finding that may otherwise appear contradictory. More contacts at higher speed can occur at the same time as shorter contact durations. Under a uniform spatial distribution, changing how quickly pairs pass through the contact region need not substantially change the fraction of time pairs occupy that region. The interacting simulations depart from this idealization through avoidance, organized movement, and finite-domain repetition. These departures are part of the result, not reasons to assume a fitted curve applies without qualification.

For planning, the useful question is therefore which outcome a change is intended to reduce. Unique contacts describe how widely a pedestrian's contact network extends. Summed pair time describes accumulated proximity under a uniform time weighting. A transmission model may weight distance, orientation, infectiousness, and simultaneous exposures differently. The different exposure mechanisms examined by Shumsky et al. provide an example of why an

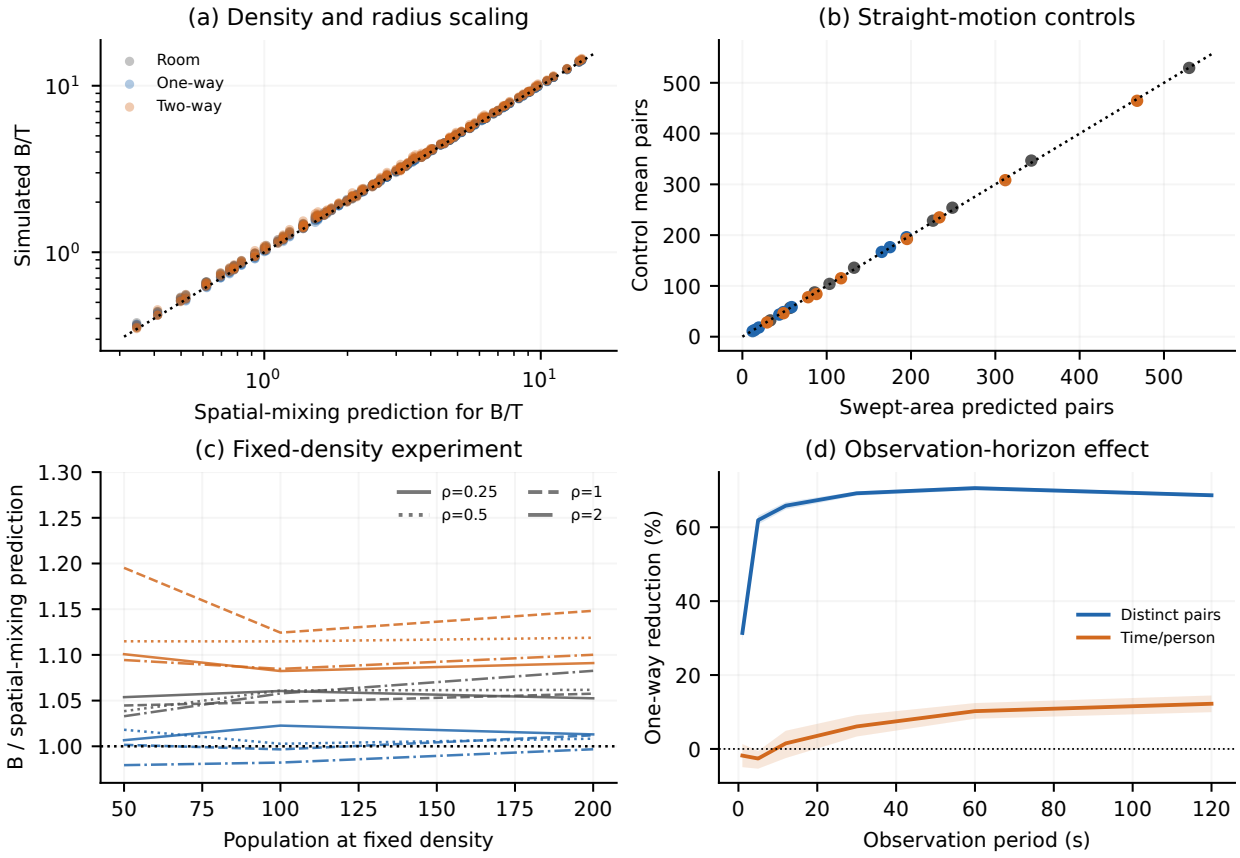

Figure 4: Additional tests of the mathematical relationships. (a) Spatial-mixing prediction versus simulated burden for $\rho \leq 0.5$. (b) Swept-area prediction versus ideal-motion controls. Dotted diagonals indicate equality. (c) Burden divided by the spatial-mixing prediction at fixed density; line styles distinguish densities 0.25, 0.5, 1, and 2. (d) One-way reductions in distinct pairs and time/person as the observation horizon changes, with paired seed-bootstrap 95% bands. Colors in (a)–(c) identify movement models.

intervention's effect need not be the same for every definition of exposure [Shumsky et al. 2021].

6.3 Limitations

Our study has several limitations. First, the periodic square has no corridor walls, doors, bottlenecks, scheduled arrivals, or destinations. Its two-way initialization allows overlap between opposing streams. A separated-lane corridor could produce different results. Complete route length and travel time must be considered in a building-level comparison, as illustrated by Romero et al. [Romero et al. 2020].

Second, the most crowded settings are not all physically plausible for the nominal pedestrian bodies. At $\rho = 8$, disks of radius 0.2 m have a combined nominal area fraction $\pi(0.2)^2\rho \approx 1.005$, already exceeding the environment area. The overlap-shrinkage rule allows such configurations numerically. Step-size sensitivity further limits their interpretation. The lower-density restriction reduces this problem but does not itself validate the model against observations.

Third, ten seeds provide a limited estimate of Monte Carlo variation. Shared seeds make matched comparisons more informative, but the narrow confidence intervals do not include uncertainty in movement rules, parameter calibration, or human compliance. The regression uses a controlled factorial grid and overlapping observations at several radii. Its high fit quality should not be interpreted as evidence from an independent sample of real buildings.

Finally, the model has no infectious pedestrians, aerosol field, respiratory orientation, masks, ventilation, or dose-response relationship. Proximity is therefore a geometric outcome. Airborne exposure depends on processes beyond a contact threshold [Bazant and Bush 2021; Vuorinen et al. 2020]. The model also does not determine whether persistent contact with one infectious individual is preferable to shorter contacts with several individuals. That question requires an explicitly specified transmission process.

6.4 Further studies

A useful next step is to replace the periodic square with measured corridor and room geometries, then compare complete trips at

matched origin–destination demand. Such experiments should include separated opposing lanes, doors, intersections, and waiting areas. Trajectory observations could calibrate realized speeds, spacing, and directional mixing before exposure is evaluated.

A second extension is to combine the contact trajectories with a distance- and time-dependent transmission model, and then with an airflow-dependent exposure model. The latter is necessary for persistent airborne contamination [Vuorinen et al. 2020]. Occupancy, routing, and air treatment could then be compared under the same infection assumptions. The present results provide reproducible contact inputs and mathematical checks for that extension.

7 CONCLUSION

Our simulations compare the contact patterns produced by room, one-way, and two-way movement. One-way movement reaches fewer distinct people, but the contacting pairs remain close for longer. The reduction in summed contact time is therefore much smaller than the reduction in contact count. We derive and test a spatial-mixing relationship that explains the strong effects of density and contact radius, together with the weaker effect of speed on cumulative burden. Additional experiments show that population comparisons must distinguish fixed area from fixed density and that contact counts depend on observation duration. The densest cases require particular numerical and physical caution. These findings support comparing pedestrian arrangements with both contact counts and accumulated time, while reserving infection-risk conclusions for models that explicitly represent transmission.

DATA AND CODE AVAILABILITY

The original source revision is `297e2dd23091` [Tang 2021]. The accompanying reproduction package contains preserved source excerpts, the original poster and draft, the headless simulator, controlled verification tests, experiment settings, per-run CSV results, analysis scripts, and figure generation. Archived and newly generated outcomes are labeled separately. Access to the original repository may require permission. The linked historical results spreadsheet was unavailable during reproduction, so the new experiments do not claim to recover the original run-level dataset. Affiliations in the author block reflect the original project.

REFERENCES

Martin Z. Bazant and John W. M. Bush. 2021. A guideline to limit indoor airborne transmission of COVID-19. *Proceedings of the National Academy of Sciences* 118, 17, Article e2018995118 (2021). https://doi.org/10.1073/pnas.2018995118

Leslie Dietz, Patrick F. Horve, David A. Coil, Mark Fretz, Jonathan A. Eisen, and Kevin Van Den Wymelenberg. 2020. 2019 Novel Coronavirus (COVID-19) Pandemic: Built Environment Considerations To Reduce Transmission. *mSystems* 5, 2, Article e00245-20 (2020). https://doi.org/10.1128/msystems.00245-20

Dirk Helbing, Lubos Buzna, Anders Johansson, and Torsten Werner. 2005. Self-Organized Pedestrian Crowd Dynamics: Experiments, Simulations, and Design Solutions. *Transportation Science* 39, 1 (2005), 1–24. https://doi.org/10.1287/trsc.1040.0108

Ioannis Karamouzas, Brian Skinner, and Stephen J. Guy. 2014. Universal Power Law Governing Pedestrian Interactions. *Physical Review Letters* 113, 23, Article 238701 (2014). https://doi.org/10.1103/physrevlett.113.238701

Lidia Morawska, Julian W. Tang, William Bahnfleth, Philomena M. Bluyssen, Atze Boerstra, Giorgio Buonanno, Junji Cao, Stephanie Dancer, Andres Floto, Francesco Franchimon, Charles Haworth, Jaap Hogeling, Christina Isaxon, Jose L. Jimenez, Jarek Kurnitski, Yuguo Li, Marcel Loomans, Guy Marks, Linsey C. Marr, Livio Mazzarella, Arsen Krikor Melikov, Shelly Miller, Donald K. Milton, William Nazaroff, Peter V. Nielsen, Catherine Noakes, Jordan Peccia, Xavier Querol, Chandra Sekhar, Olli Seppanen, Shin-ichi Tanabe, Raymond Tellier, Kwok Wai Tham, Pawel Wargocki, Aneta Wierzbicka, and Maosheng Yao. 2020. How can airborne transmission of COVID-19 indoors be minimised? *Environment International* 142, Article 105832 (2020). https://doi.org/10.1016/j.envint.2020.105832

Van Romero, William D. Stone, and Julie Dyke Ford. 2020. COVID-19 indoor exposure levels: An analysis of foot traffic scenarios within an academic building. *Transportation Research Interdisciplinary Perspectives* 7, Article 100185 (2020). https://doi.org/10.1016/j.trip.2020.100185

Robert A. Shumsky, Laurens Debo, Rebecca M. Lebeaux, Quang P. Nguyen, and Anne G. Hoen. 2021. Retail store customer flow and COVID-19 transmission. *Proceedings of the National Academy of Sciences* 118, 11, Article e2019225118 (2021). https://doi.org/10.1073/pnas.2019225118

Charles Tang. 2021. Viral-Transmission-Pedestrian-Model. https://github.com/charlestang06/Viral-Transmission-Pedestrian-Model Source commit 297e2dd230911290a4b21327ec8cfefc28f0cfe4, 23 July 2021. Accessed 25 November 2026; repository access may be required.

Charles Tang, Archanaa S. Krishnan, and Patrick Schaumont. n.d.. Why One-Way Hallways Are Safer Than Two-Way Hallways. (n.d.). Unpublished research poster supplied with the project materials; preserved in the accompanying reproduction package.

Ville Vuorinen, Mia Aarnio, Mikko Alava, Ville Alopaeus, Nina Atanasova, Mikko Auvinen, Nallannan Balasubramanian, Hadi Bordbar, Panu Erasto, Rafael Grande, Nick Hayward, Antti Hellsten, Simo Hostikka, Jyrki Hokkanen, Ossi Kaario, Aku Karvinen, Ilkka Kivisto, Marko Korhonen, Risto Kosonen, Janne Kuusela, Sami Lestinen, Erkki Laurila, Heikki J. Nieminen, Petteri Peltonen, Juho Pokki, Antti Puisto, Peter Raback, Henri Salmenjoki, Tarja Sironen, and Monika Osterberg. 2020. Modelling aerosol transport and virus exposure with numerical simulations in relation to SARS-CoV-2 transmission by inhalation indoors. *Safety Science* 130, Article 104866 (2020). https://doi.org/10.1016/j.ssci.2020.104866